# Dielectric effect on electric fields in the vicinity of the metal-vacuum-dielectric junction

Chung, Moon S; Mayer, Alexander; Miskovsky, Nicholas; Weiss, Brock L; Cutler, Paul H

*Published in:*
Ultramicroscopy

*DOI:*
10.1016/j.ultramic.2012.12.014

*Publication date:*
2013

*Document Version*
Early version, also known as pre-print

# Dielectric effect on electric fields in the vicinity of the metal-vacuum-dielectric junction

M. S. Chung[a*], A. Mayer[b], N. M Miskovsky[c], B. L.Weiss[c], and P. H. Cutler[c]
[a] Department of Physics, University of Ulsan, Ulsan 680-749, Korea
[b] FUNDP – University of Namur, Rue de Bruxelles 61, B-5000 Namur, Belgium
[c] Department of Physics, The Pennsylvania State University, University Park, PA 16802, USA

The dielectric effect was theoretically investigated for the electric field in the vicinity of a junction of metal, dielectric, and vacuum. The assumption of the two-dimensional symmetry of junctions leaded to a simple analytic form and to a systematic numerical calculation for the field. The electric field obtained for the triple junction was found to be enhanced and reduced according to the certain criteria determined by the contact angles along with the dielectric constant. Further numerical calculations of the dielectric effect exhibit that an electric field can experience a larger enhancement or reduction for a quadruple junction than for the triple one. It was also found that even though it changes slowly in comparison with the shape effect, the dielectric effect was noticeably large over the entire change of shape.

PACS: 79.70.+q, 85.45.Db, 77.22.Jp

Keywords: triple junction, field enhancement, dielectric effect, metal-dielectric contact

## 1. Introduction

Dielectrics are usually considered to reduce the electric field intensities. For a long time, however, strongly enhanced electric fields have often been observed in the phenomenon of electron emission avalanche or breakdown in the vicinity of the metal-dielectric contact [1-5]. Such an unexpected field enhancement, called the triple junction effect, must be due to

* Electronic mail: mschung@ulsan.ac.kr

dielectric in contact with metal (see Fig. 1). Two significant experiments to reveal the dielectric effect were made by the Geis group [4,6]. In 1977, they reported the enhanced field emission when the diamond portion of the triple junction was extended into the vacuum. Several years later, they observed the field emission which continued even after the bias was removed. Ma and Sudarshan [7,8] found that voids at the contact were crucial in vacuum insulation breakdown. The contact angle of the junction was considered to play a role in the enhancement mechanism [9-14]. Schächter [15] first used a two-dimensional model to obtain the theoretical result that the field emission current density was proportional to the dielectric constant for a specific triple junction.

The field enhancement at the triple junction is different from that produced by a protrusion or a sharpening of the metallic edge [16]. The electric field is enhanced or reduced according to the angular configuration of the triple junction [12-14]. The value of the dielectric constant is a factor to determine the magnitude of the enhancement. This implies that both the magnitude and direction of polarization are involved to determine the enhancement of the electric field. Thus it is interesting to find what configuration yield the largest dielectric enhancement through polarization with the triple junction as a basis. One of most probable candidates is a quadruple junction even though it may not appear as often as a triple junction (see Fig. 1). According to the previous work [17], we have found that a certain type of quadruple junction yields the larger dielectric effect than the triple junction. Even though it is not experimentally confirmed yet, the use of the triple or quadruple junction may lead to a new type of cold electron source. In addition, a deeper understanding of the dielectric effect may be used to avoid an avalanche of electron emission or breakdown. Thus we need to make a systematic approach to describe the field behavior in the region near the contact of metal and dielectric.

2. Metal-vacuum-dielectric triple junctions

As seen in Fig. 1, the metal-layer contact has several configurations of junction at which metal, vacuum, and dielectric meet [6]. Since it is a layer-by-layer contact, the junction structure has a relatively large longitudinal dimension in comparison with the facial size. Thus we assume that junctions have the two-dimensional symmetry. As a triple junction, we can consider the axis of a cylinder composed of three portions of metal, vacuum, and dielectric meet, as seen in Fig. 2. As far as the electric field in the vicinity of the junction is concerned, the cylinder plays the same role as the real triple junction configuration. It is supposed that the cylinder has a length of $\ell \approx 1$ mm and a radius of $R \approx 1$ μm ($R << \ell$).

Now we use the polar coordinates ($r$, $\theta$). The two-dimensional portions of metal, vacuum and dielectric are given by angles $\alpha$, $\theta_1$ and $\theta_2$, respectively. The electric potential $\Phi$ is given by the solution of the two-dimensional Laplace equation

$$r\frac{\partial}{\partial r}\left(r\frac{\partial \Phi}{\partial r}\right)+\frac{\partial^2 \Phi}{\partial \theta^2}=0 \qquad (1)$$

In general, the solution is written in the form $\Phi=\sum_n r^{\nu_n}(A_n \sin \nu_n\theta + B_n \cos \nu_n\theta)$, where $r$ is the distance from the junction and $A_n$ and $B_n$ arbitrary constants. Since $r$ is limited to the vicinity of the junction, i.e., $r << R$, only the lowest-power term is dominant. Then $\Phi$ is given by [18]

$$\Phi_1 = A_1 r^{\nu} \sin \nu\theta, \qquad 0<\theta<\theta_1 \ \text{(vacuum)}, \qquad (2)$$

$$\Phi_2 = A_2 r^{\nu} \sin \nu(\theta_t-\theta), \ \theta_1<\theta<\theta_1+\theta_2=\theta_t=2\pi-\alpha \ \text{(dielectric)}, \qquad (3)$$

where subscripts 1 and 2 refer to the vacuum and dielectric regions, respectively and we put $\nu = \nu_1$, being positive. From Eqs. (2) and (3), the electric field magnitude $F = |\nabla\Phi|$ is given by

$$F_1 = A_1 \nu r^{\nu-1}, \qquad 0 < \theta < \theta_1 \quad \text{(vacuum)}, \tag{4}$$

$$F_2 = A_2 \nu r^{\nu-1}, \qquad \theta_1 < \theta < \theta_t \quad \text{(dielectric)}. \tag{5}$$

Both magnitudes $F_1$ and $F_2$ are independent of the angle variable $\theta$ and their behaviors are majorly characterized by $\nu$ only.

Now we use the boundary conditions which are the continuities of both $\Phi$ and $D_\theta = (\varepsilon / r)(\partial\Phi / \partial\theta)$ at $\theta = \theta_1$. The two obtained relations are

$$\varepsilon \tan \nu\theta_1 = -\tan \nu\theta_2 . \tag{6}$$

$$A_2 / A_1 = \sin \nu\theta_1 / \sin \nu\theta_2 \equiv \eta \tag{7}$$

Equation (6) becomes the very equation for $\nu$. Equation (7) is used to evaluate $F_2$ since $\eta$ is equal to the field ratio $F_2 / F_1$ for $r_1 = r_2$.

The analytic solutions for $\nu$ are easily found in the two limiting cases of $\varepsilon$ = 1 and $\varepsilon \to \infty$. For $\varepsilon$ =1 (in the absence of dielectric), Eq. (6) is satisfied at

$$\nu = \nu_0 = \pi / \theta_1 = \pi / (2\pi - \alpha) . \tag{8}$$

This is $\nu$ just for the contact of metal and vacuum [18]. Next we rewrite Eq. (6) into the form $1/\varepsilon = \tan(\pi - \nu\theta_1)/\tan\nu\theta_2$. In the limit $\varepsilon \to \infty$, the right side is zero when the numerator is zero or when the denominator becomes infinity. Then we have two solutions of which the lower one is

$$\nu_\infty / \nu_0 = \begin{cases} 1/(\theta_1/\theta_t) = 1/(1-\theta_2/\theta_t), & 0 < \theta_2/\theta_t < 1/3 \\ 0.5/(\theta_2/\theta_t), & 1/3 < \theta_2/\theta_t < 1 \end{cases}. \qquad (9)$$

We plot the curve of $\nu_\infty$ versus $\theta_2$ in Fig. 3. Each coordinate is normalized with $\nu_0$ and $\theta_t$ The reason is that even though both $\nu_0$ and $\nu_\infty$ are a function of $\alpha$, $\nu_\infty/\nu_0$ is independent of $\alpha$. We do not need to calculate $\nu$ for all values of $\alpha$ but only one value, say $\alpha = \pi$. It is seen that $\nu_\infty/\nu_0$ has the maximum of 1.5 at $\theta_2/\theta_t$=1/3 and the minimum of 0.5 at $\theta_2/\theta_t$=1. Then $\nu_\infty$ has the minimum of 0.25 since $\nu_0$ has the minimum of 0.5, at $\alpha$=0. It is interesting to see the difference metal and dielectric of $\varepsilon = \infty$. Metal gives one curve (dotted line) whereas dielectric of $\varepsilon = \infty$ gives two curves (solid line).

For real dielectrics of $1 < \varepsilon < \infty$, we make numerical calculations of Eq. (6) to obtain $\nu(\varepsilon)$, $\nu$ in short, as a function of $\theta_2$, $\alpha$ and $\varepsilon$. We take $\varepsilon$=5.7 (diamond), 10.4 (GaN), 100, and 1000. The obtained $\nu$ are plotted in Fig. 4. We also insert $\nu$ for metal (dashed line) for comparison. We have $\nu_0 < \nu < \nu_\infty$ or $\nu_\infty < \nu < \nu_0$ according to the value of $\theta_2$. That is, $\nu$ can be smaller or larger than $\nu_0$. The electric field becomes stronger or weaker in the presence of dielectric than that in the absence of dielectric.

Both the maximum and minimum points depend on $\varepsilon$. As $\varepsilon$ increases from 1 to $\infty$, the maximum position $(\theta_2/\theta_t)_{max}$ moves from 1/4 to 1/3 whereas the minimum $(\theta_2/\theta_t)_{min}$

moves from 3/4 to 1.0. On the other hand, the maximum value $(\nu/\nu_0)_{max}$ moves from 1.0 to 3/2 whereas the minimum $(\nu/\nu_0)_{min}$ moves from 1.0 to 1/2. It is worthwhile to note that the shape of the curve is asymmetry under reversal. We choose $\varepsilon$=5.7 (diamond) and 10.4 (GaN) for real materials, and $\varepsilon$=100 and 1000 for large values. The $\nu$ is very close to $\nu_\infty$ for $\varepsilon$=100 and $\nu$ is almost the same as $\nu_\infty$ for $\varepsilon$=1000. However, there is one thing to mention. The $\nu/\nu_0$ becomes 1 just at $\theta_2 = \theta_t$ for $\varepsilon$ as large as possible in Fig 4, whereas $\nu_\infty/\nu_0$ is 0.5 in Fig. 4. Two are not the same. We should be back to Eq. (6), which leads to the value $\nu = \nu_0$ at $\theta_2$=0, $\theta_t/2(=\theta_1)$, and $\theta_t$, regardless of $\varepsilon$. No change in $F$ is made when the field region is occupied with vacuum or dielectric only, or is divided equally. It is then required that $\nu/\nu_0$=1 at $\theta_2 = \theta_t$, even for an extremely large value of $\varepsilon$.

At this point, we have to stress the two properties important for the field behavior even though they were mentioned in the previous work [12]. First, it depends on the ratio $\theta_2/\theta_t$ (or the ratio $\theta_2/\theta_1$) whether $\nu$ is larger than $\nu_0$ or not. Simply, $\nu$ is larger than $\nu_0$ for $\theta_2 < \theta_t/2$ (i.e., $\theta_2 < \theta_1$) and is smaller for $\theta_2 > \theta_t/2$ (i.e., $\theta_2 > \theta_1$). This implies that F is enhanced (or reduced) for $\theta_2$ larger (or smaller) than $\theta_1$. At $\theta_2 = \theta_1$, $\nu$ is equal to $\nu_0$, implying no enhancement of $F$ at all. Secondly, the value of $\varepsilon$ is only the factor to determine the shape of $\nu/\nu_0$ versus $\theta_2/\theta_t$. As $\varepsilon$ increases, it has the higher peak and deeper valley, meaning a larger enhancement or reduction in the field [12-14].

## 3. Quadruple junctions

### 3.1 Metal-vacuum-dielectric-vacuum quadruple junctions

For a deeper understanding of the dielectric effect, we consider the metal-vacuum-dielectric-vacuum (MVDV) quadruple junction formed by introducing another vacuum portion between metal and dielectric in the triple junction (see Figs. 1, 2, and 5). Symbols $\alpha$,

$\theta_1$, $\theta_2$ and $\theta_3$ indicate the angles subtended by metal, vacuum, dielectric, and vacuum, respectively. In the same way as done for the triple junction, we make the two-dimensional treatments to find the solution, $\Phi$, of the Laplace equation. In the region near the junction, $\Phi$ can be given in the forms [17,18]

$$\Phi_1 = A_1 r^{\nu} \sin \nu\theta, \qquad 0 \le \theta \le \theta_1 \ \text{(vacuum)}, \tag{10}$$

$$\Phi_2 = r^{\nu} (A_2 \sin \nu\theta + B_2 \cos \nu\theta), \quad \theta_1 \le \theta \le \theta_1 + \theta_2 \ \text{(dielectric)}, \tag{11}$$

$$\Phi_3 = A_3 r^{\nu} \sin \nu(2\pi - \alpha - \theta), \qquad \theta_1 + \theta_2 \le \theta \le \theta_1 + \theta_2 + \theta_3 = \theta_t \ \text{(vacuum)}, \tag{12}$$

where the subscript refers to the region. In each region, the electric field is given in the form

$$F_1 = A_1 \nu r^{\nu-1}, \qquad 0 \le \theta \le \theta_1 \ \text{(vacuum)}, \tag{13}$$

$$F_2 = (A_2^{\,2} + B_2^{\,2})^{1/2} \ \nu r^{\nu-1}, \quad \theta_1 \le \theta \le \theta_1 + \theta_2 \ \text{(dielectric)}, \tag{14}$$

$$F_3 = A_3 \nu r^{\nu-1}, \qquad \theta_1 + \theta_2 \le \theta \le \theta_1 + \theta_2 + \theta_3 = \theta_t \ \text{(vacuum)}. \tag{15}$$

Using the boundary conditions of both $\Phi$ and $\partial\Phi/\partial\theta$ at $\theta = \theta_1$ and $\theta_1 + \theta_2$, we have four relations for five unknowns, $\nu$ and four coefficients $A_i$ (i=1, 2, and 3) and $B_2$. Three are the expressions of three coefficients in terms of the rest, say $A_2$. The fourth is the transcendental equation for $\nu$ [17]:

$$\frac{(1-\varepsilon)\tan \nu\theta_1}{1+\varepsilon \tan^2 \nu\theta_1} = \frac{\tan \nu(\theta_1+\theta_2) + \varepsilon \tan \nu\theta_3}{1-\varepsilon \tan \nu(\theta_1+\theta_2)\tan \nu\theta_3}. \tag{16}$$

It seems that $\theta_1$ and $\theta_3$ are not exchangeable in Eq. (16). However, the exchange of $\theta_1$ and $\theta_3$ does not give rise to any difference in $\nu$. As expected so, Eq. (16) reduces to Eq. (6) when $\theta_3$=0.

We make numerical calculations of Eq. (16) to obtain $\nu$ as a function of $\theta_2$ for several values of $\theta_3$. The obtained results are shown in Fig. 6 for $\theta_3$ = 0 (a triple junction), $30^o$, $60^o$, $90^o$, $120^o$, $150^o$ (asymmetric), and $\theta_1$ (symmetric). The two curves of $\theta_3$=$30^o$ and $120^o$, or $60^o$ and $120^o$ are complementary but are not symmetric. The reason is that $\theta_3$ is fixed whereas $\theta_1 (= 2\pi - \alpha - \theta_3 - \theta_2)$ varies with varying $\theta_2$. As seen in Fig. 6, we have two interesting properties for the MVDV junction. First, all $\nu$'s are lower than those for the triple junction. This implies that the MVDV quadruple junction can yield more enhancement of field than the triple junction. Second, $\nu$ for the symmetric quadruple junction of $\theta_3 = \theta_1$ is the entire loci of valleys for asymmetric junctions. This means that the symmetric MVDV junction always yields the lowest $\nu$ at given $\theta_2$ and then the largest enhancement of $F$. It is also interesting that $\nu$ for the symmetric MVDV junction has the minimum at $\theta_2 = \theta_t / 2$, irrespective of values of $\varepsilon$. It is recalled that for the triple junction, it moves to the larger $\theta_2$ as $\varepsilon$ increases.

3.2 Metal-dielectric-vacuum-dielectric quadruple junctions

Alternatively, we consider the metal-dielectric-vacuum-dielectric (MDVD) quadruple junction obtained by inserting an additional dielectric portion between metal and vacuum in the triple junction (see Figs. 1, 2, and 5). This structure may be the case that void exists on the side of dielectric at the triple junction. Symbols $\alpha$, $\theta_3$, $\theta_1$, and $\theta_2$ represent the angles subtended by metal, dielectric, vacuum, and dielectric, respectively. Numbering begins at 3. This choice is made so that the case of $\theta_3$=0 always represents the same triple junction as treated before. Since similar arguments is applicable in obtaining $\Phi$, we write

$\Phi_3 = A_3 r^{\nu} \sin \nu\theta$ for $0 \le \theta \le \theta_3$ , $\Phi_1 = r^{\nu} (A_1 \sin \nu\theta + B_1 \cos \nu\theta)$ for $\theta_3 \le \theta \le \theta_3 + \theta_1$ , and $\Phi_2 = A_2 r^{\nu} \sin \nu(2\pi - \alpha - \theta)$ for $\theta_3 + \theta_1 \le \theta \le \theta_3 + \theta_1 + \theta_2$, where subscripts 3, 1, and 2 refer to the regions. The use of the boundary conditions at $\theta = \theta_3$ and $\theta_3 + \theta_1$ yields the associated transcendental equation

$$\frac{(1-\varepsilon)\tan \nu\theta_3}{\varepsilon + \tan^2 \nu\theta_3} = \frac{\varepsilon \tan \nu(\theta_3 + \theta_1) + \tan \nu\theta_2}{-\varepsilon + \tan \nu(\theta_3 + \theta_1)\tan \nu\theta_2} . \qquad (17)$$

,

As expected, Eqs. (16) and (17) are similar in form. The difference comes from the different composites and numbering.

Numerical calculations of Eq. (17) are carried out to obtain $\nu$ as a function of $\theta_1$ for several values of $\theta_3$. As seen in Fig. 7, we have two interesting properties for the MDVD junction. First, all $\nu$'s are higher than those for the triple junction. This implies that the field can be more largely reduced for the MDVD junction than for the triple junction. Second, $\nu$ for the quadruple junction of $\theta_3 = \theta_2$ is the entire loci of peaks for asymmetric junctions of given $\theta_3$. This means that the symmetric MDVD junction always yields the highest $\nu$ at given $\theta_2$. It is interesting that $\nu$ for the symmetric MDVD junction has the maximum at $\theta_2 = \theta_t / 2$, irrespective of $\varepsilon$.

## 4. Electric fields and enhancements

### 4.1 Electric fields for the triple junction

It is supposed that a free negative charge $Q$ is distributed on the surface of the metal (see Fig. 2). Since the surface charge density is given by the normal component of displacement,

we use Eqs. (4) and (5) to derive $Q = -\ell\, R^{\nu}\,(1+\eta\varepsilon)A_1$. The field energy $W$ is calculated to be $W = \nu R^{2\nu}\,\ell\,(\theta_1 + \eta^2\,\varepsilon\,\theta_2)A_1^{\,2}/16\pi$. Then we have the potential [12,15]

$$V = 2W/Q = -\frac{\nu}{8\pi}\,R^{\nu}\,\frac{\theta_1 + \eta^2\,\varepsilon\,\theta_2}{1+\eta\,\varepsilon}\,A_1. \tag{18}$$

$V$ is regarded as the electric potential imposed on the metal with free charge $Q$. Combining Eqs. (4), (5), (7), and (18), we have

$$F_1(r) = 8\pi\left(\frac{1+\eta\,\varepsilon}{\theta_1 + \eta^2\,\varepsilon\,\theta_2}\right)\left(\frac{r}{R}\right)^{\nu-1}\left(\frac{-V}{R}\right), \tag{19}$$

$$F_2 = \eta\,F_1(r). \tag{20}$$

Now we define the reference field $F_0$ as $F_1$ when dielectric is replaced with vacuum. At $\varepsilon$=1, where $\theta_2$=0, $\theta_1 = \theta_t$, $\eta$=1 and $\nu = \nu_0$, Eq. (19) becomes

$$F_0 = 16\,\nu_0\left(\frac{r}{R}\right)^{\nu_0-1}\left(\frac{-V}{R}\right). \tag{21}$$

The field enhancement $\beta$ is defined as the ratio of the two fields, $F_1$ and $F_0$:

$$\beta(r) = F_1(r)/F_0(r) = 0.5\left(\frac{1+\eta\,\varepsilon}{1+(\eta^2\,\varepsilon-1)\,\theta_2/\theta_t}\right)\left(\frac{R}{r}\right)^{\nu_0-\nu}. \tag{22}$$

It is clear that Eq. (22) yields $\beta = 1$ at $\varepsilon = 1$. For $\varepsilon > 1$, $\beta$ is larger or smaller than unity according to the value of $\nu / \nu_0$, or $\theta_2 / \theta_1$. That is, $\beta$ is smaller (or larger) than unity for $\theta_2 < \theta_1$ (or $\theta_2 > \theta_1$). It is found that the prefactor in Eq. (22) varies approximately from unity to 5.5 over the entire range of $\theta_2$. We choose R = 1μm and r =0.1 nm to make numerical calculations of $\beta$ in the enhancement region (see Fig. 8). For $\varepsilon = 5.7$ (dotted line), we have the minimum enhancement $\beta_{min} \approx 0.17$ at $\theta_2 / \theta_t \approx 0.29$ and the maximum enhancement $\beta_{max} \approx 19.8$ at $\theta_2 / \theta_t \approx 0.91$. For $\varepsilon = 10.4$ (solid line), we have $\beta_{min} \approx 0.12$ at $\theta_2 / \theta_t \approx 0.30$ and the maximum $\beta_{max} \approx 47.1$ at $\theta_2 / \theta_t \approx 0.93$. This is the enhancement $\beta$ of vacuum field $F_1$ (blue line). The dielectric field $F_2$ has the enhancement $\eta\beta$ (red line), which is smaller $\beta$. As seen in Figs. 4 and 8, both $\nu_{min}$ and $\beta_{max}$ do not take places at the same $\theta_2 / \theta_t$. The $\beta$ has the maximum at a little larger $\theta_2$ than $\nu$, due the prefactor of Eq. (22). It is worthwhile to mention that all the associated extrema $\nu_{min}$, $\beta_{max}$, $F_{1,max}$ and $F_{2,max}$ lie in the region $0.75 < \theta_2 / \theta_t < 1.0$.

The $\varepsilon$-dependence of $\beta_{max}$ is shown more clearly in Fig. 9. It seems that $\beta_{max}$ increases almost linearly with increasing $\varepsilon$. The slope depends on $\alpha$ and r. We take the values of r =0.1 and 1.0 nm with the fixed value of R =1 μm. As $\varepsilon$ increases from 1 to 100 (not shown here), $\beta_{max}$ increases from 1.0 to 122.5 for $\alpha = 0$ and r =1.0 nm (red dashed line), from 1.0 to 153.2 for $\alpha = 0$ and r =0.1 nm (red solid line), and from 1.0 to 669.4 for $\alpha = 180^o$ and r =0.1 nm (blue solid line). The $\beta_{max}$ becomes very large for large $\varepsilon$, especially at small r and $\alpha = 180^o$. Two plots of $\alpha = 0$ and r =0.1 nm (red solid line), and $\alpha = 90^o$ and r =1.0 nm (green dashed line) coincide accidently.

Figure 10 shows the $\alpha$-dependence of $\beta_{max}$ and $F_0$. The $\alpha$-dependence reflects the curvature of the metallic shape. From Eq. (22), we have the exponent $\nu_0 - \nu = \nu_0(1 - \nu / \nu_0)$.

The value $\nu/\nu_0$ depends on the dielectric property only. In contrast, $\nu_0$ depends on the curvature of the metallic shape. Thus the $\alpha$-dependent enhancement comes majorly from the $\alpha$-dependence of $F_0$. Irrespective of dielectric, $F_0$ increases with decreasing $\alpha$. In the presence of dielectric, $\beta$ increases with increasing $\alpha$. Since $F_1 = \beta F_0$, there is the competition between the two factors in determining $F_1$ ( and $F_2$) as $\alpha$ varies. To figure out the curvature-dependence of both enhancements, we have made numerical calculations of $F_0$, $F_{1,max}$ and $F_{2,max}$ as a function of $\alpha$. The numerical values of F are calculated by setting $16\pi V/R = 4.0$ and then varies with the applied bias V. We use the arbitrary unit for F just to know the relative magnitudes.

As $\alpha$ increases from 0 to $180^o$, $F_0(r)$ decreases from 63.7 to 1.27 (50 times smaller), irrespective of $\varepsilon$. Instead, $\beta_{max}$ increases from 7.77 to 19.8 (2.5 times larger) for $\varepsilon = 5.7$ and from 15.0 to 47.1 (3.1 times larger) for $\varepsilon = 10.4$. This implies that $F_0$ changes more rapidly with $\alpha$ than $\beta$ or $\eta\beta$. As a result, both $F_{1,max}$ and $F_{2,max}$ are shown to increase with decreasing $\alpha$. However, the dielectric enhancement is still significant or large over all $\alpha$. The dielectric effect is not just apparently visible because it changes slowly in comparison with the shape effect.

4.2 Electric fields for the quadruple junction

As discussed in section 3, the MVDV junction is effective in enhancing the field whereas the MDVD in reducing the field. In the current work, we consider the MVDV junction. We apply the same calculation scheme as used for the triple junction to obtain

$$\beta(r) = F_1(r)/F_0(r) = 0.5\left(\frac{\eta_1(\eta_1+\eta_2)\theta_t}{\eta_1^{\,2}\theta_1 + \varepsilon(1+\eta_2^{\,2})\theta_t + \eta_3^{\,2}\theta_3}\right)\left(\frac{R}{r}\right)^{\nu_0-\nu}, \qquad (23)$$

where $\eta_1 = A_1/A_2$, $\eta_2 = B_2/A_2$, $\eta_3 = A_3/A_2$. All $\eta_i$ (i=1, 2 and 3) are obtained using the boundary condition [17]. Two $\beta(r)$ given by Eqs (22) and (23) are the same in form and are different in the configuration-dependence.

For the symmetric quadruple junction of $\theta_3 = \theta_1$, we make Eq. (23) to obtain $\beta(r)$ as a function of $\theta_2/\theta_t$ for $\varepsilon$=5.7. The results are shown in Fig. 11. We consider r=0.1 (solid line) and 1.0 nm (dashed line). We also plot $\beta(r)$ for the triple junction for comparison. We have the maximum enhancement $\beta_{max}$=21.8 and 66.1 for r=1.0 and 0.1 nm, respectively. Those are 12.0 and 19.8 for the triple junction. The $\beta_{max}$ for the symmetric quadruple junction are 2 or 3 times larger than those for the triple junction. The dielectric effect is more effective for the quadruple junction.

The difference between enhancements for the triple and quadruple junctions supports the reason that the electric field is enhanced or reduced by the polarization of dielectric. In the absence of dielectric, the surface charge is distributed so that the potential is constant over the metallic surface, resulting in the $\alpha$-dependence of $F_0$. If dielectric is introduced to be in contact with metal, then the charge on the metal causes dielectric to polarize. In turn, the free surface charge on metal is also redistributed under the influence of polarization charges. The magnitude and direction of polarization depends on the contact angles of the constituents. If polarization charges attract free surface charges to the junction, then more free charges are accumulated near the junction. The field becomes strong. The strong field produces larger polarization. This process goes on until the perfect polarization of dielectric is reached. As a result, the very strong is formed due to dielectric for the triple and quadruple junctions in the

region near the junction of metal, vacuum, and dielectric.

## 5. Conclusions

We described the electric field in the vicinity of metal-dielectric contact with vacuum.. The assumption of the two-dimensional symmetry of junctions leaded to the formulation of the field enhancement due to dielectric. For the triple junction, the electric field was found to be enhanced and reduced according to the contact angle ratio as well as the dielectric constant. It was found that a certain type of quadruple junction yielded a larger enhancement than the triple junction. It was noted that the enhancement of the electric field at the metal-dielectric contact is the product of the two enhancements due to dielectric and the shape of the metallic emission portion. Such an field enhancement may be large enough for the strange triple junction phenomenon such as the vacuum or dielectric breakdown.

## ACKNOWLEDGMENT

This research was supported by Mid-carrier Research Program through the NRF grant funded by the MEST (Grant No. R01-2008-000-20025-0). This research was also supported by the Basic Science Research Program through National Research Foundation of Korea funded by the MEST (Grant No. 2011-0009500).

## REFERENCES

[1] A. Watson, J. Appl. Phys. 38 (1967), 2019.

[2] G. N. Fursei and P. N. Vorontsov-Vel’yaminov, Sov. Phys. Tech. Phys. 12 (1968), 1370.

[3] R. V. Latham, Vacuum 32 (1982), 137.

[4] M. W. Geis, N. N. Efremow, Jr., K. E. Krohn, J. C. Twichell, T. M. Lyszczarz, R. Kalish, J. A. Greer and M. D. Taber, Lincoln Lab. J. 10 (1997), 3.

[5] 14N. M. Jordan, Y. Y. Lau, D. M. French, R. M. Gilgenbach, and P. Pengvanich, J. Appl. Phys. 102 (2007), 03301.

[6] M. W. Geis, S. Deneault, K. E. Krohn, M. Marchant, T. M. Lyszczarz, and D. L. Crooke, Appl. Phys. Lett. 87 (2005), 192115.

[7] X. Ma and T. S. Sudarshan, J. Vac. Sci. Technol. B 19 (2001), 683.

[8] X. Ma and T. S. Sudarshan, J. Vac. Sci. Technol. B 16 (1998), 745.

[9] T. Takuma, IEEE Transaction on Electric Insulation 26 (1991), 500.

[10] O. Yamamoto and T. Takuma, Electrical Eng. Japan 131 (2000), 1.

[11] B. Techaumnat, S. Hamada, T. Takuma, J. Electrostatics 56 (2002), 67.

[12] M. S. Chung, B.-G. Yoon, P. H. Cutler and N. M. Miskovsky, J. Vac. Sci. Technol. B 22 (2004), 1240.

[13] M. S. Chung, T. S. Choi, and B.-G. Yoon, Appl. Surf. Sci. 251 (2005), 177.

[14] M. S. Chung, S. C. Hong, P. H. Cutler and N. M. Miskovsky, B. L. Weiss, and A. Mayer., J. Vac. Sci. Technol. B 24 (2006), 909.

[15] L. Schächter, Appl. Phys. Lett. 72 (1998), 421.

[16] P. H. Cutler, N. M. Miskovsky, P. B. Lerner, and M. S. Chung, Appl. Surf. Sci. 146 (1999), 126.

[17] M. S. Chung, B,-G. Yoon, P. H. Cutler and N. M. Miskovsky, B. L. Weiss, and A. Mayer., J. Vac. Sci. Technol. B 24 (2010), C2A94.

[18] J. D. Jackson, J. D. Jackson, Classical Electrodynamics, 3rd ed., John Wiley & Sons, New York, 1999.

Figure Captions

Fig. 1 Triple and quadruple junctions formed on an interface. There may exist a triple junction of metal-vacuum-dielectric (small blue circle) and quadruple junctions of metal-vacuum-dielectric-vacuum (red large circle) and metal-dielectric-vacuum-dielectric (red dotted circle) [6].

Fig. 2 Triple junctions made by Geis et al. [4](a) for experiment and suggested by authors (b) for calculation. Two are reduced to the two-dimensional junction (c), where the coordinate origin is taken at the triple junction (d). The contact angles of metal, vacuum, and dielectric are given by $\alpha$, $\theta_1$, and $\theta_2$, respectively. The cylinder is considered to have the radius $R \approx 1\mu m$ and the length $\ell \approx 1mm$.

Fig. 3 Enhancement parameter $\nu_\infty$ for the triple junction. The inset shows the plot of $\nu_0$ versus $\theta_1$ for the metal-vacuum junction ($\theta_2$=0). The dotted line represents $\nu$ when dielectric portion is metallic.

Fig. 4 Enhancement parameter $\nu$ for $1<\varepsilon<\infty$. We take $\varepsilon$=5.7 (diamond) and 10.4 (GaN), 100, 1000. As $\varepsilon$ increases, $\nu$ has higher peaks and lower valleys and both peaks and valleys move toward the larger $\theta_2$.

Fig. 5 Cylindrical quadruple junctions. Additional portion, vacuum (a) or dielectric (b), is added to the triple junction. Symbol $\theta_3$ always indicates the angle subtended by the additional portion. .

Fig. 6 Enhancement parameter $\nu$ for the metal-vacuum-dielectric-vacuum quadruple junction. We take $\theta_3$=0(triple junction), $30^o$, $60^o$, $90^o$, $120^o$, $150^o$, and $\theta_1$ (symmetric).

Fig. 7 Enhancement parameter $\nu$ for the metal-dielectric-vacuum-dielectric quadruple junction. We take $\theta_3$=0(triple junction), $30^o$, $60^o$, $90^o$, $120^o$, $150^o$, and $\theta_1$ (symmetric).

Fig. 8 Field enhancements of vacuum and dielectric fields for the triple junction. We take $\varepsilon$=5.7 (dashed line) and 10.4 (solid line). The enhancement, $\beta$, for the vacuum field $F_1$ (blue line) is larger than that for the dielectric field $F_2$ (red line).

Fig. 9 Plot for $\beta_{max}$ versus $\varepsilon$. The maximum enhancement $\beta_{max}$ is shown as a function of $\varepsilon$ for r=0.1 (solid line) and 1.0 nm (dashed line) and $\alpha$=0, $90^o$, and $180^o$. It is seen that $\beta_{max}$ increases almost linearly with increasing $\varepsilon$. The plot for $\alpha$=0 and r=0.1 nm is overlapped on that for $\alpha=90^o$ and r=1.0 nm.

Fig. 10 Shape-dependence of the field and the enhancement. As $\alpha$ varies from 0 to $180^o$, $F_0$ decreases rapidly while $\beta$ increases slowly. Thus both $F_1$ (blue line) and $F_2$ (red line) are shown to follow the trend of $F_0$. We take $\varepsilon$=5.7 (dashed line) and 10.4 (solid line).

Fig. 11. Field enhancement for the symmetric quadruple junction. The symmetric metal-vacuum-dielectric-vacuum quadruple junction (blue line) yields the larger enhancement than the triple junction (red line). We take We take r=0.1 (solid line) and 1.0 nm (dashed line).

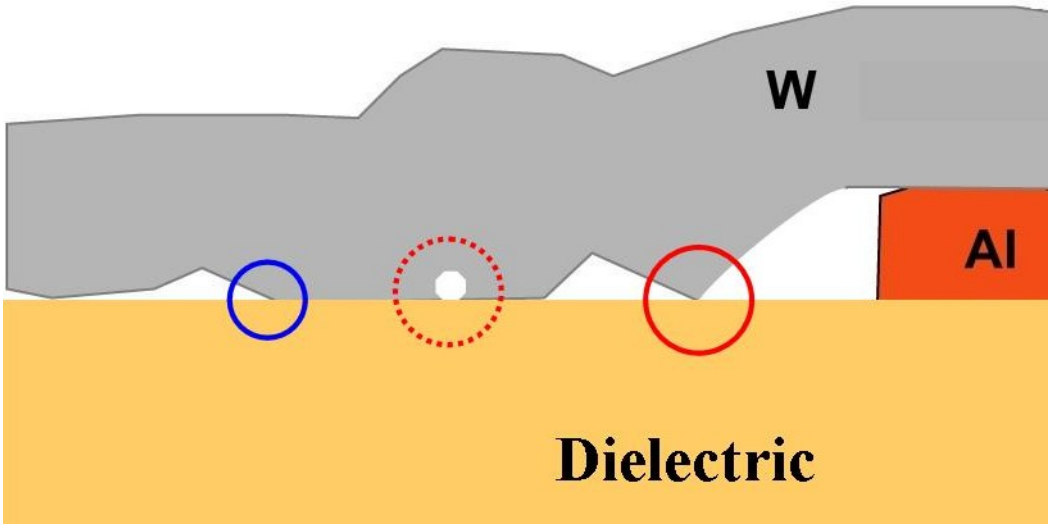


Fig. 1

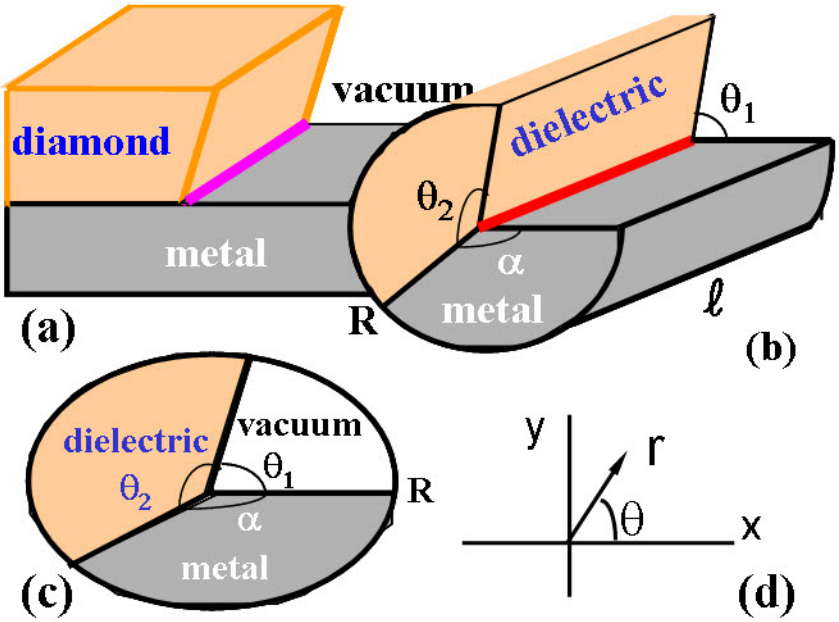
diamond
vacuum
dielectric
θ1
θ2
metal
α
metal
R
ℓ
(a)
(b)
dielectric
vacuum
θ2
θ1
α
R
metal
(c)
y
r
θ
x
(d)

Fig. 2

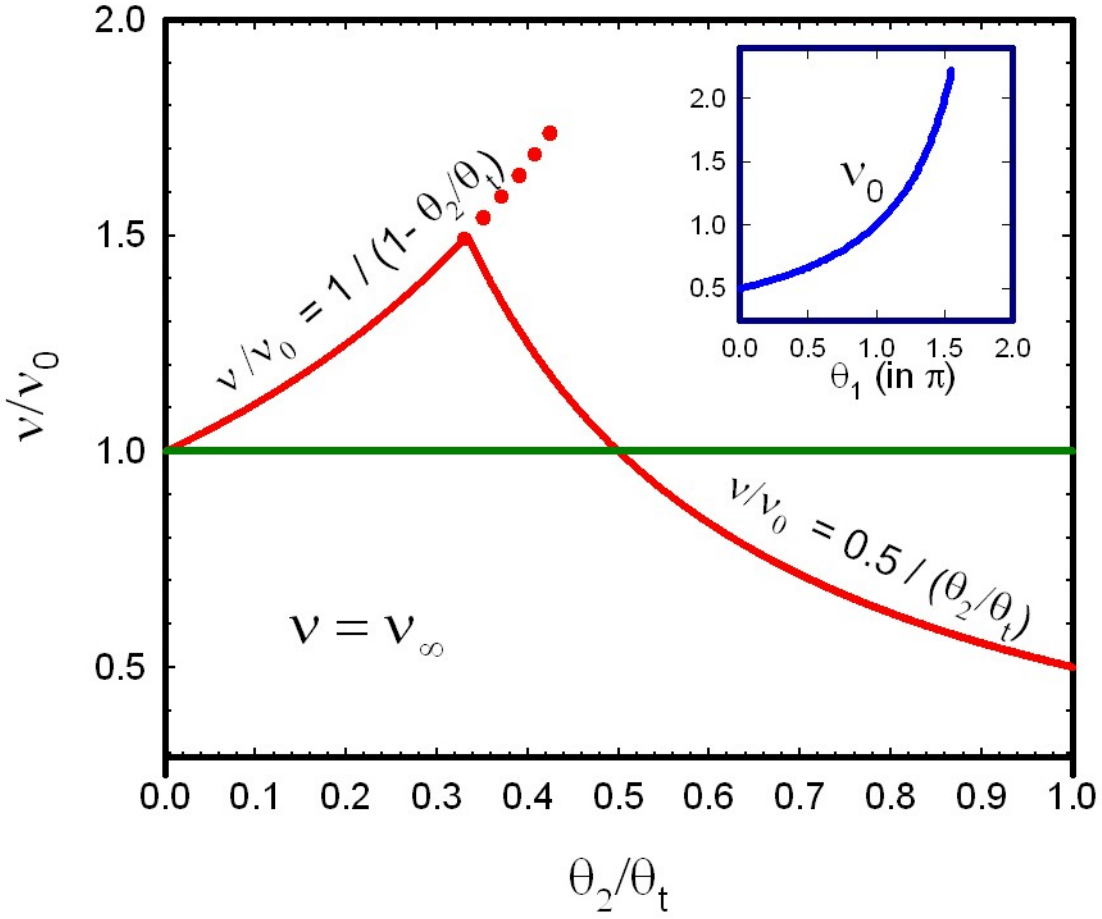
2.0
1.5
1.0
0.5
ν/ν0
0.0 0.1 0.2 0.3 0.4 0.5 0.6 0.7 0.8 0.9 1.0
θ2/θt
ν/ν0 = 1 / (1- θ2/θt)
ν/ν0 = 0.5 / (θ2/θt)
ν = ν∞
ν0
2.0
1.5
1.0
0.5
0.0 0.5 1.0 1.5 2.0
θ1 (in π)

Fig. 3

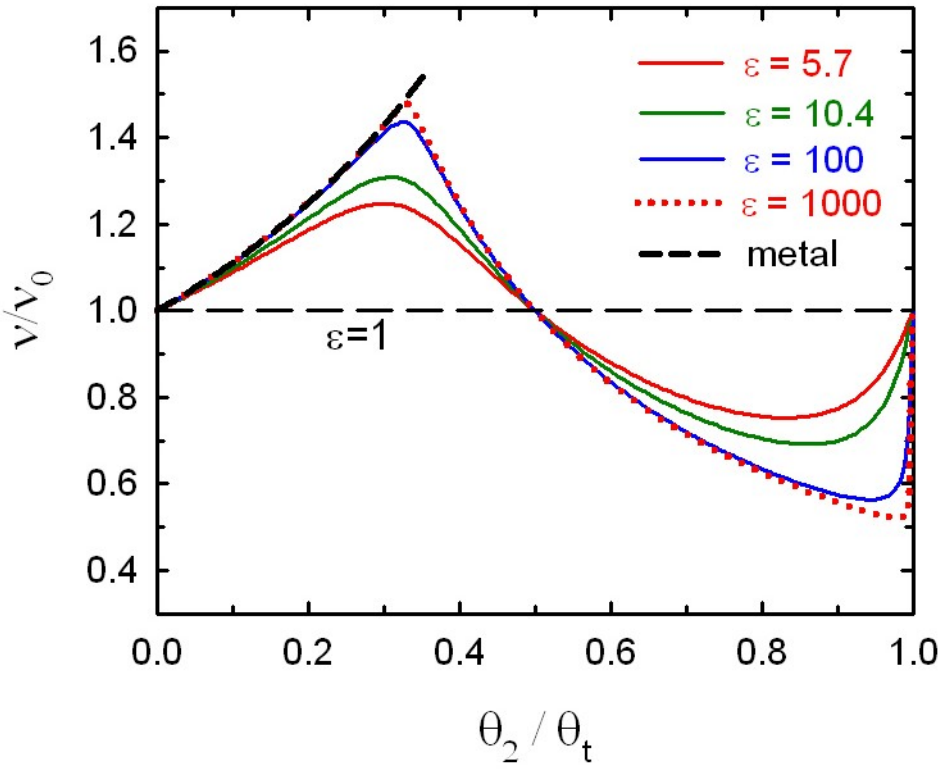
1.6
1.4
1.2
1.0
0.8
0.6
0.4
0.0
0.2
0.4
0.6
0.8
1.0
v/v0
θ2 / θt
ε = 5.7
ε = 10.4
ε = 100
ε = 1000
metal
ε=1

Fig. 4

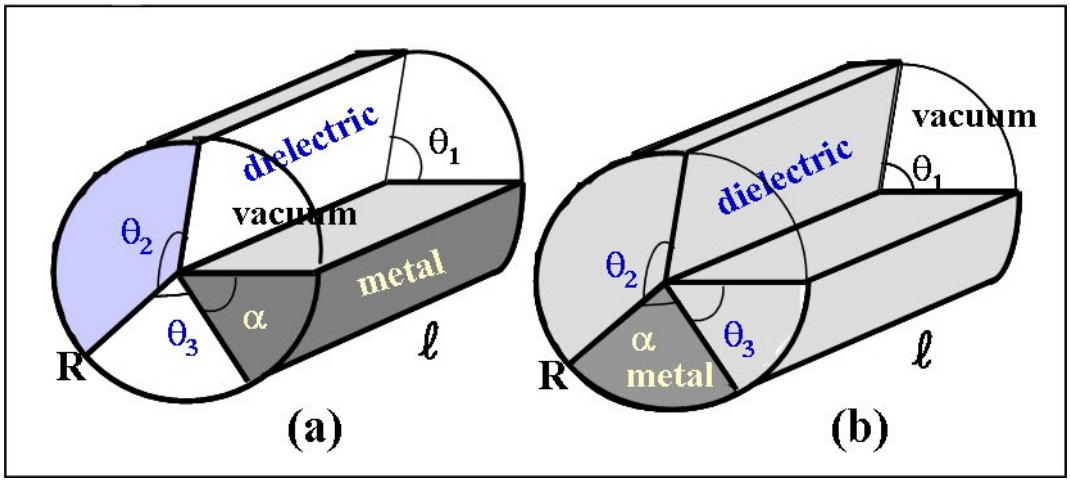
dielectric
vacuum
θ1
θ2
θ3
α
metal
R
ℓ
(a)
vacuum
dielectric
θ1
θ2
α
metal
θ3
R
ℓ
(b)

Fig. 5

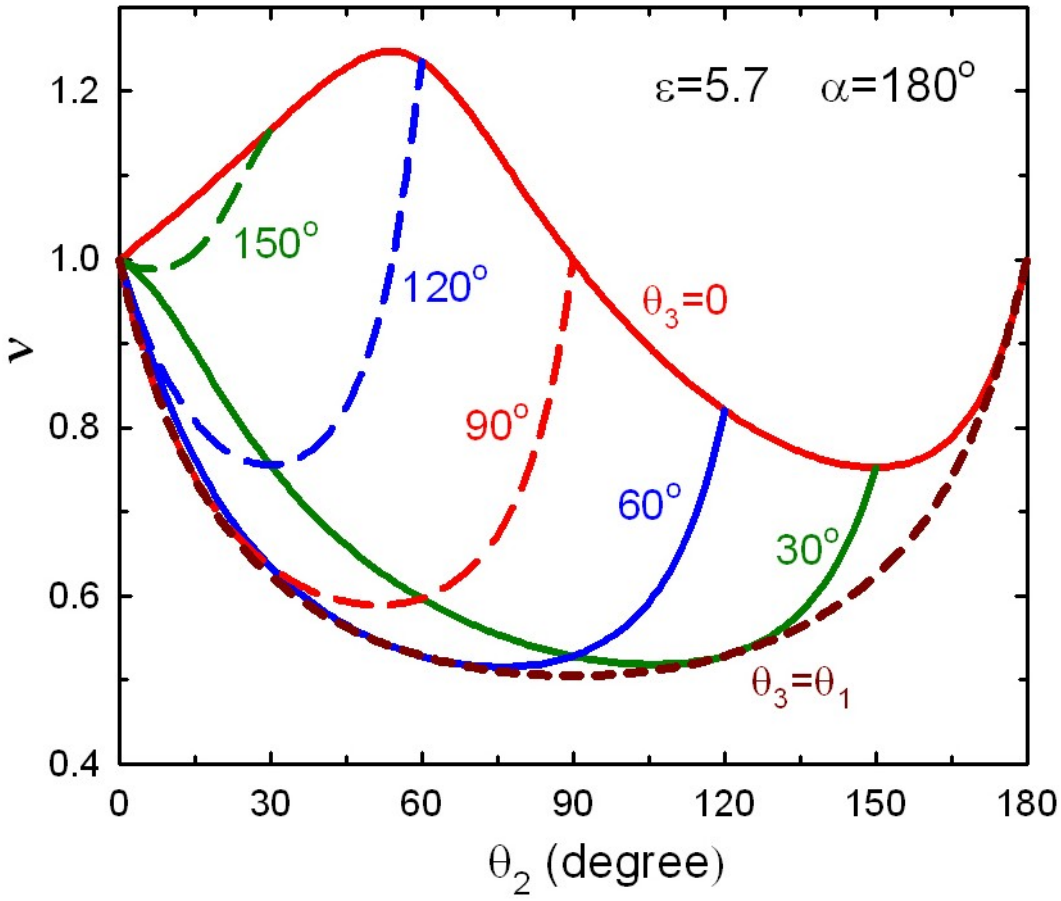
ε=5.7 α=180°
150°
120°
θ3=0
90°
60°
30°
θ3=θ1
ν
θ2 (degree)
1.2
1.0
0.8
0.6
0.4
0
30
60
90
120
150
180

Fig. 6

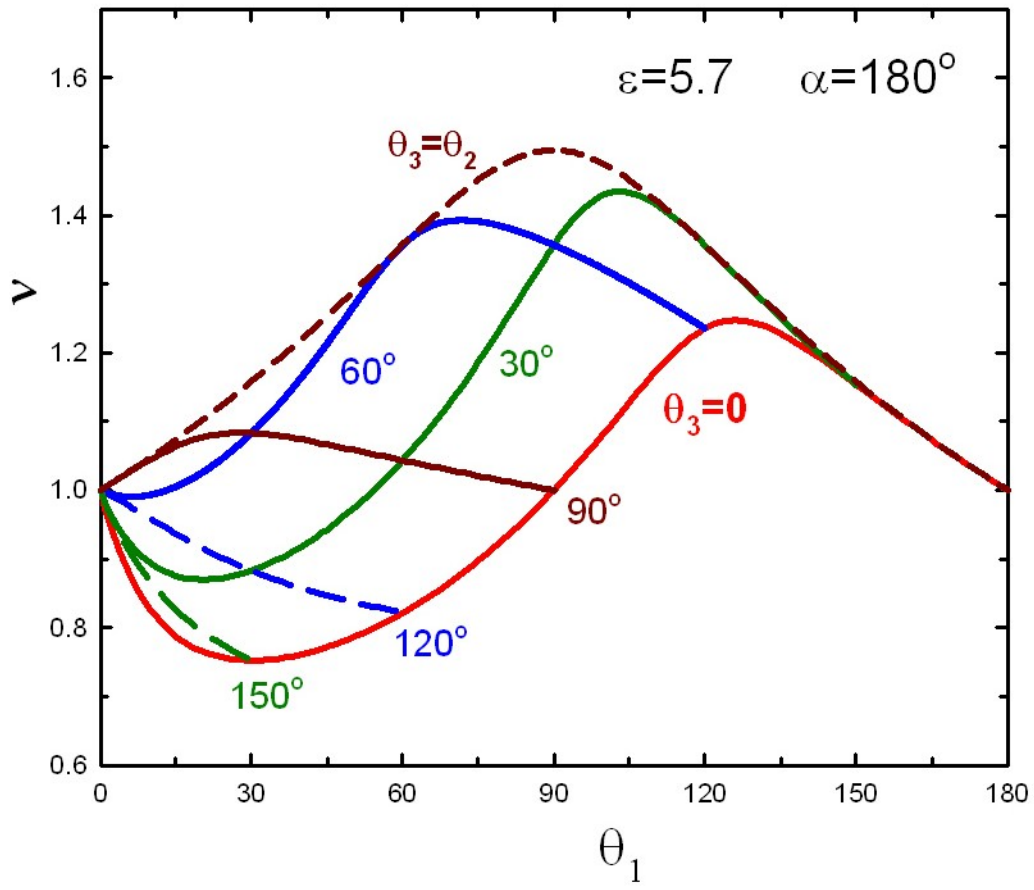
ε=5.7 α=180°
θ3=θ2
60°
30°
θ3=0
90°
120°
150°
ν
θ1
1.6
1.4
1.2
1.0
0.8
0.6
0
30
60
90
120
150
180

Fig. 7

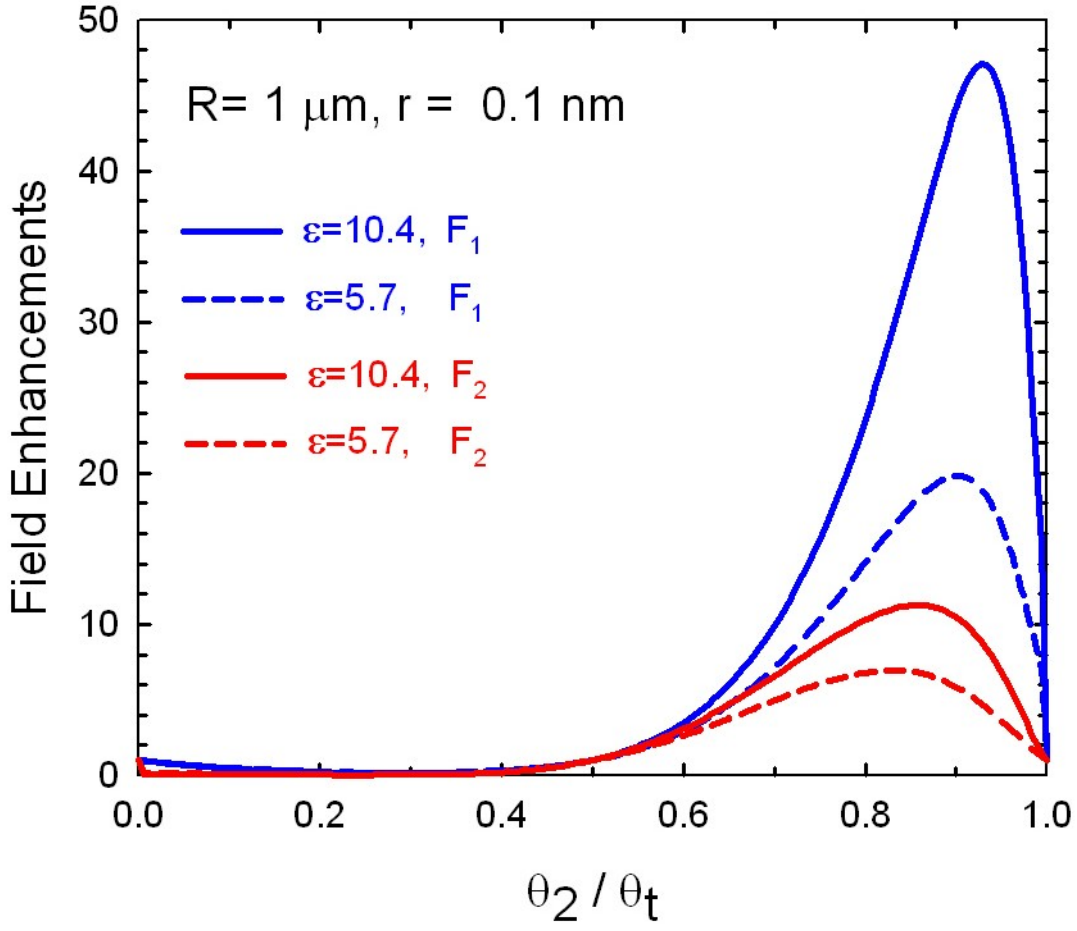
R= 1 μm, r = 0.1 nm
ε=10.4, F1
ε=5.7, F1
ε=10.4, F2
ε=5.7, F2
Field Enhancements
θ2 / θt
0
10
20
30
40
50
0.0
0.2
0.4
0.6
0.8
1.0

Fig. 8

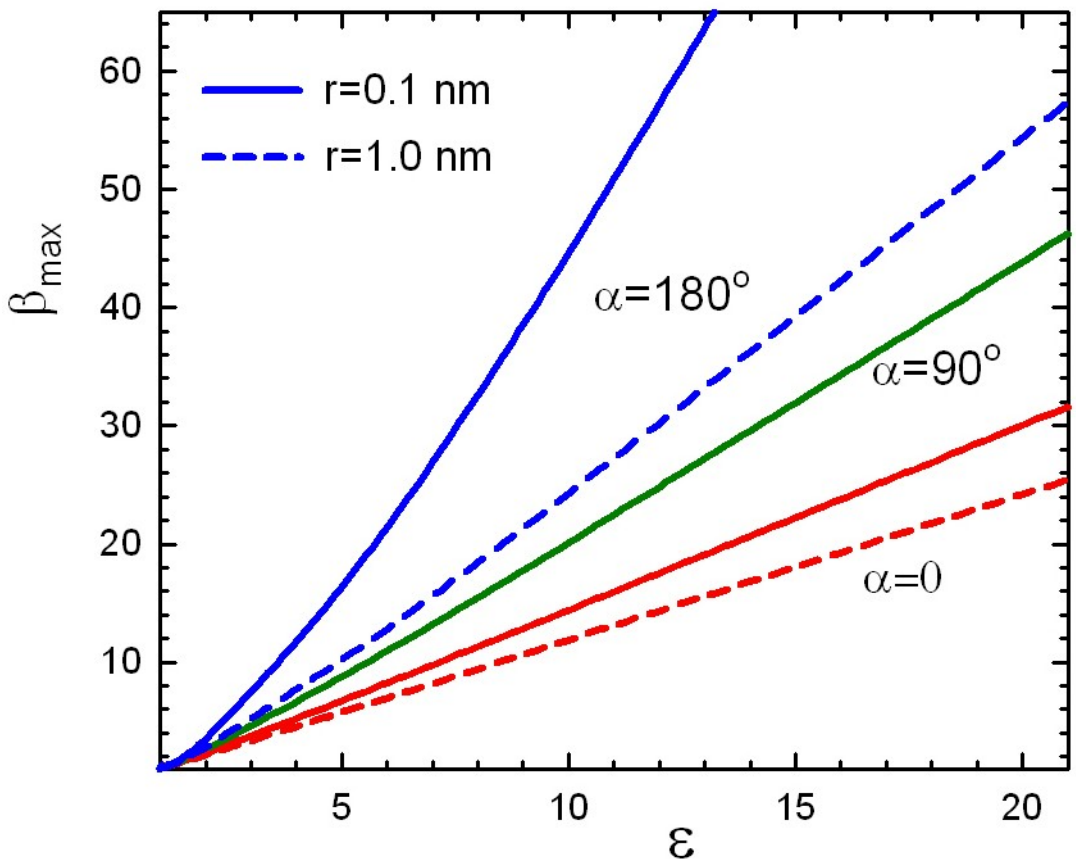


Fig. 9

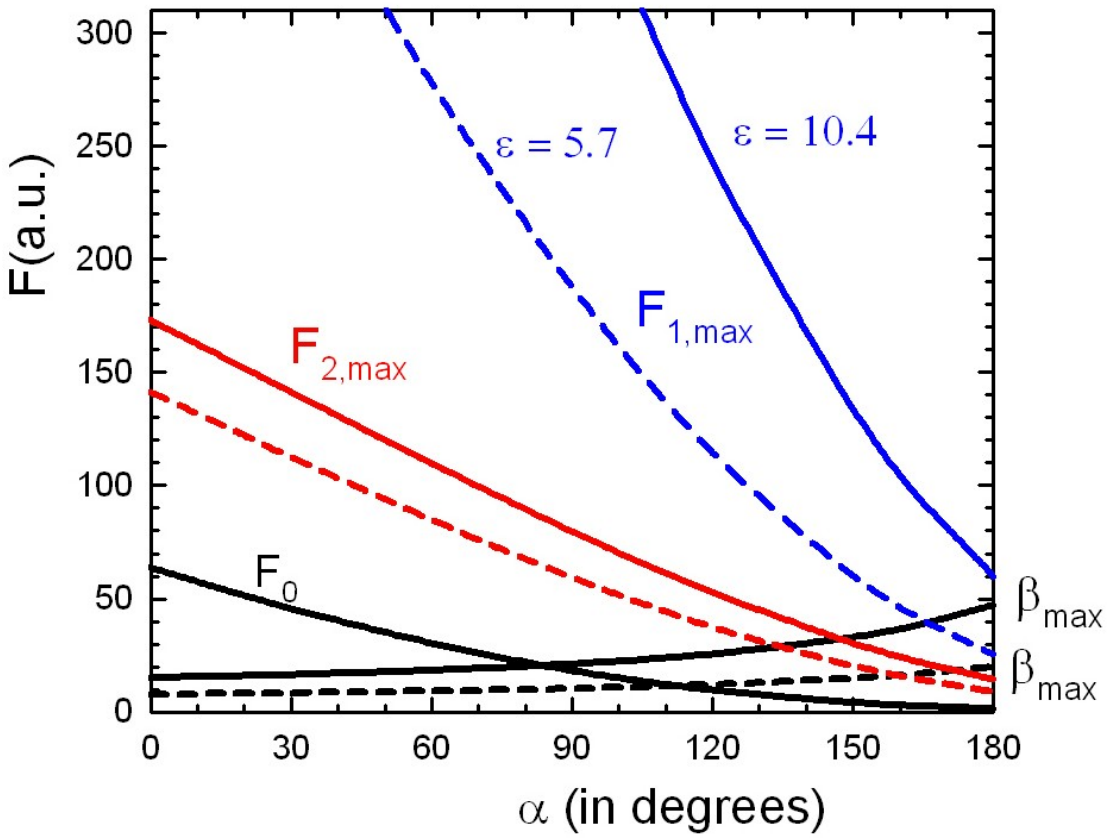
F(a.u.)
300
250
200
150
100
50
0
0
30
60
90
120
150
180
α (in degrees)
ε = 5.7
ε = 10.4
F1,max
F2,max
F0
βmax
βmax

Fig. 10

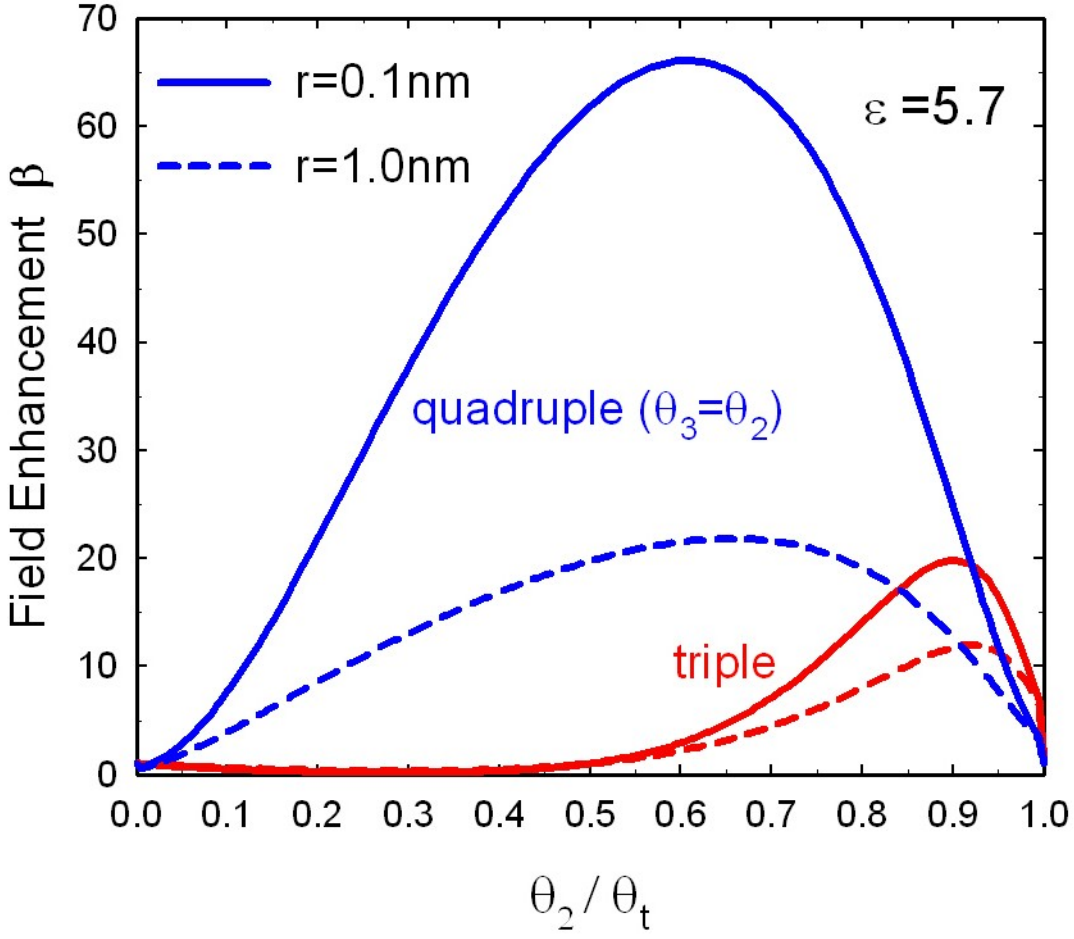
r=0.1nm
r=1.0nm
ε =5.7
quadruple (θ3=θ2)
triple
Field Enhancement β
θ2 / θt
0
10
20
30
40
50
60
70
0.0
0.1
0.2
0.3
0.4
0.5
0.6
0.7
0.8
0.9
1.0

Fig. 11